

Extensive entanglement between coupled Tomonaga-Luttinger liquids in and out of equilibrium

Taufiq Murtadho¹, Marek Gluza¹, Nelly H. Y. Ng^{1,2}

¹ School of Physical and Mathematical Sciences, Nanyang Technological University, 637371, Singapore

² Centre for Quantum Technologies, Nanyang Technological University Singapore, 50 Nanyang Avenue, Singapore 639798, Singapore.

E-mail: fiqmurtadho@gmail.com, nelly.ng@ntu.edu.sg

Abstract. Quantum entanglement exists in nature but is absent in classical physics, hence it fundamentally distinguishes quantum from classical theories. While entanglement is routinely observed for few-body systems, it is significantly more challenging to witness in quantum many-body systems. Here, we theoretically study entanglement *between* two parallel and spatially separated Tomonaga-Luttinger liquids (TLLs) partitioned *along* the longitudinal axis. In particular, we focus on 1D Bose gases as a realization of TLLs and investigate two experimentally relevant situations: tunnel-coupled gases at finite temperatures and after coherent splitting. In both scenarios, we analytically calculate the logarithmic negativity and identify a threshold temperature below which the system is entangled. Notably, this threshold temperature is accessible in near-term coherent splitting experiments. Furthermore, we investigate the crossover between quantum and classical correlations in the vicinity of the threshold temperature by comparing logarithmic negativity with mutual information. We argue that the initial mutual information established by the coherent splitting is conserved in TLL dynamics, thus preventing certain generalized Gibbs ensembles from being reached during prethermalization. Moreover, both logarithmic negativity and mutual information are found to scale extensively with the subsystem's length. Although the ground-state entanglement between coupled TLLs has been predicted to be extensive, this setting is largely overlooked compared to other partitions. Our work extends the study of entanglement between coupled TLLs to finite temperatures and out-of-equilibrium regimes, and provides a strategy towards experimental detection of extensive entanglement in quantum many-body systems at finite temperatures.

1. Introduction

Entanglement is a type of quantum correlation that has no analogue in classical physics, hence it serves as a fundamental signature to distinguish quantum from classical systems [1]. In addition to its fundamental importance, entanglement is also a key resource for quantum information processing [2]. Entanglement has been routinely observed and utilized in well-controlled few-body systems [3, 4], but detecting and characterizing entanglement in quantum many-body systems, in particular those described by effective quantum field theories (QFTs), is challenging. Such many body-systems involve many degrees of freedom and therefore have a potential to host a macroscopic amount of entanglement. At the same time, experimental access is typically limited to coarse-grained observables. The immensity of the Hilbert space versus the limited number of measurement settings makes it difficult to experimentally witness entanglement [5, 6], especially at finite temperatures [7, 8].

For many-body systems constrained to one-dimension (1D), their low-energy behaviors are effectively described by the Tomonaga-Luttinger liquid (TLL) [9]. When two such TLLs are arranged in parallel and coupled through tunneling, they form a quantum simulator for the sine-Gordon model [10–12]—a paradigmatic example of a strongly interacting integrable field theory important for various physical phenomena of interest [13]. This model is experimentally realized in parallel 1D Bose gases on an atom chip, where thousands of ultracold atoms are trapped in an elongated potential with a double-well transverse cross section [11, 12, 14–19]. Advances in coherent control [20–22] and Gaussian tomography [23, 24] for this setup have allowed experiments to probe quantum information in and out of equilibrium [19, 25], and yet experimental study of entanglement in this setup is scarce.

One of the main bottlenecks is that most results in the literature of entanglement for 1D systems focus on partitioning across the 1D axis (also known as the transversal cut, see Fig. 1) [26–31], dividing the total length of the system into non-overlapping segments. It is a ubiquitous expectation that the ground state entanglement entropy for this partition follows the area law in the presence of a spectral gap [30], which in 1D implies that the entanglement does not grow with longer subsystem length; for a gapless system the entanglement grows with subsystem’s length albeit only logarithmically [29]. While parallel 1D Bose gases experiments confirm the area law for mutual information at finite temperatures [19], entanglement with transversal

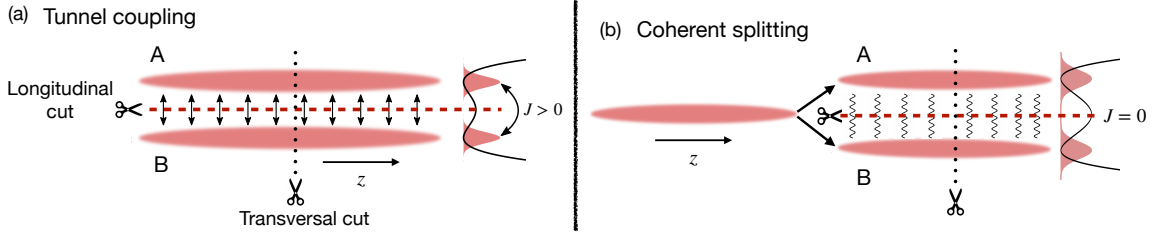


Figure 1. Two parallel 1D quasicondensates A and B , extended along the z -axis, each with its own phase and density fluctuations. While typically the system is partitioned across the z -axis (black dotted line, transversal cut), we partition the system along the z -axis (red dashed line, longitudinal cut). (a) Coupling between A and B is introduced in the Hamiltonian through tunneling, whose strength is tunable by adjusting the height of the double-well barrier. (b) Initial correlation between A and B is dynamically induced by coherently splitting the trap from a single to double-well.

partition has not been reported, possibly because only microscopic amounts can be naturally generated and it is quickly diluted by thermal noise [5–8, 19].

In this work, we highlight a better strategy to observe entanglement, i.e. across the *longitudinal cut* (dashed line in Fig. 1) which partitions the system along the 1D axis, dividing it into two transversally separated 1D gases. This partitioning is the more natural strategy for experimentally observing entanglement, since the mechanisms for generating strong correlations are well understood. For example, correlation can be introduced via tunnel-coupling interaction, implemented by adjusting the height of the double-well barrier (Fig. 1a) [11, 12, 18, 19], or by coherently splitting the potential from a single to double-well (Fig. 1b) [16, 17, 32–35]. Indeed, recent experiments have witnessed entanglement in the longitudinal partition through number squeezing [36]. Previously, progress was limited by a lack of experimental readout techniques, but recent advances including outcoupling measurement [37] and common phase interferometry [38] have overcome this barrier, providing new experimental windows to probe entanglement. However, surprisingly little is known about the theory behind entanglement in the longitudinal partition.

Beyond its experimental relevance, analyzing the longitudinal cut is also of theoretical interest. It enables quantum simulation of entanglement between multiple quantum fields coexisting and interacting in a common (1+1D) spacetime [39–43],

which is not as well understood as the more conventional spatial partition of a single quantum field. In condensed matter physics, this setting is also relevant for studying systems with ladder geometries [44–46], particularly to study the interplay between inter-chain and intra-chain coupling. Previous works [47, 48] have shown that the ground state entanglement entropy between two coupled TLLs scales linearly with subsystem’s length, which they characterize as ‘boundary law’. We remark that in this case, boundary law is not synonymous with the standard area law since, due to embedding in higher dimension, the boundary size scales as the subsystem’s volume. Thus, coupled TLLs contain an extensive yet spatially structured entanglement arising from local interactions, which distinguish them from generic many-body excited states also obeying volume law scaling but with a high degree of scrambling [49, 50].

To our knowledge, the entanglement between two parallel coupled TLLs has not been characterized beyond the ground state. We address this gap by investigating entanglement and mutual information in realistic experimental scenarios: at finite temperatures and after coherent splitting. We specify the conditions and the parameter regimes where entanglement can be observed and show that these are achievable in near-term experiments.

The paper is organized as follows. After this introduction, we present preliminaries in Sec. 2 which include the Hamiltonian of coupled 1D Bose gases (Subsec. 2.1), covariance matrix for Gaussian fields (Subsec. 2.2), and procedure to compute entanglement and mutual information of mixed Gaussian states (Subsec. 2.3). In Sec. 3, we present our results on logarithmic negativity and mutual information of tunnel-coupled system at finite temperatures. Then, in Sec. 4 we extend our analysis to a non-equilibrium state by considering the system after coherent splitting. Finally, we present the summary and outlook in Sec. 5.

2. Preliminaries

2.1. Coupled 1D Bose gases Hamiltonian

We consider two parallel 1D Bose gases with repulsive contact interaction, extended along the z -axis which we will refer to as the *longitudinal* direction. Each 1D gas is described by a bosonic field operator $\hat{\psi}^a(z)$ with superscript $a, b \in \{A, B\}$ labeling the two gases (Fig. 1). We will use a small letter in the superscript to represent

an abstract label while a capital letter is reserved for a specific subsystem. At low energies, the fluctuation of the field operator can be decomposed into phase $\hat{\phi}^a(z)$ and density fluctuations $\delta\hat{n}^a(z)$ via the Madelung transformation

$$\hat{\psi}^a(z) = e^{i\hat{\phi}^a(z)} \sqrt{n_{1D} + \delta\hat{n}^a(z)}, \quad (1)$$

with n_{1D} being the mean density. For simplicity, we assume identical box potential for both gases, giving a uniform and equal mean density. The phase and density fluctuations are conjugate variables satisfying canonical commutation relation

$$[\delta\hat{n}^a(z), \hat{\phi}^b(z')] = i\delta(z - z')\delta_{ab}, \quad (2)$$

with $\delta(z - z')$ being understood as a smeared δ -function within the healing length $\xi_h = \hbar/\sqrt{mgn_{1D}}$, below which the low-energy theory is expected to break down [51]. Here \hbar is the reduced Planck constant, m is the atomic mass, and g is the interatomic repulsion strength.

The low-energy Hamiltonian governing the dynamics of these fluctuations is given by the Tomonaga-Luttinger liquid (TLL) model, which in the quasicondensate regime is given by [52]

$$\hat{H}_{\text{TLL}}^a = \int_0^L dz \left[\frac{\hbar^2 n_{1D}}{2m} (\partial_z \hat{\phi}^a(z))^2 + \frac{g}{2} (\delta\hat{n}^a(z))^2 \right]. \quad (3)$$

We are interested in the entanglement between the two TLLs. A common way to introduce correlation between them is to add a tunnel-coupling of the form $-\hbar J(\hat{\psi}^{A\dagger}\hat{\psi}^B + \text{h.c.})$ to the Hamiltonian, with J being the tunneling strength. This interaction is experimentally realized by adjusting the height of the double-well barrier. Such tunneling induces a non-linear interaction of the form

$$\hat{H} = \hat{H}_{\text{TLL}}^A + \hat{H}_{\text{TLL}}^B - 2\hbar J n_{1D} \int \cos \left[\hat{\phi}^A(z) - \hat{\phi}^B(z) \right] dz \quad (4)$$

in the low-energy model, assuming small density fluctuations $\delta\hat{n}^a(z) \ll n_{1D}$.

The coupled Hamiltonian (4) is usually treated by expressing the fields in the symmetric (+) and antisymmetric (−) basis

$$\hat{\phi}^\pm(z) = \frac{1}{\sqrt{2}} \left[\hat{\phi}^A(z) \pm \hat{\phi}^B(z) \right] \quad \delta\hat{n}^\pm(z) = \frac{1}{\sqrt{2}} \left[\delta\hat{n}^A(z) \pm \delta\hat{n}^B(z) \right], \quad (5)$$

which preserves the canonical commutation relation. We emphasize that the antisymmetric (relative) and symmetric (common) phases $\hat{\phi}^\pm(z)$ commute and can be measured simultaneously at single-shot level in experiments [38, 53, 54], thereby providing access to the individual phase profiles $\hat{\phi}^{A,B}(z)$ up to a constant. In the \pm basis, the Hamiltonian decouples into Luttinger liquid in the symmetric sector and a sine-Gordon model in the antisymmetric sector [10, 11]

$$\begin{aligned}\hat{H} &= \hat{H}_{\text{TLL}}^+ + \hat{H}_{\text{TLL}}^- - 2\hbar J n_{\text{1D}} \int \cos \left[\sqrt{2} \hat{\phi}^-(z) \right] dz \\ &\approx \hat{H}_{\text{TLL}}^+ + \hat{H}_{\text{TLL}}^- + 2\hbar J n_{\text{1D}} \int \left(\hat{\phi}^-(z) \right)^2 dz.\end{aligned}\quad (6)$$

In Eq. (6), we used a harmonic approximation for the cosine term valid in the strong coupling regime (when J dominates over other couplings), giving a Gaussian model for the coupled systems. In this paper, we focus on this Gaussian limit where tunneling only adds a mass term to the antisymmetric sector, realizing the Klein-Gordon field [19, 24, 55].

The underlying tunnel-coupled Hamiltonian can be diagonalized using a Bogoliubov transformation, resulting in two-species bosonic theory comprising a massless mode (+) and a massive (−) mode. The diagonalized Hamiltonian of the non-zero momentum modes is given by

$$\hat{H} \approx \sum_{k \neq 0} \varepsilon_k^+ (\hat{b}_k^+)^{\dagger} \hat{b}_k^+ + \varepsilon_k^- (\hat{b}_k^-)^{\dagger} \hat{b}_k^-, \quad (7)$$

where k are the momentum of the quasiparticles, and \hat{b}_k^\pm are the associated bosonic annihilation operators. For a free dispersion of the form $E_k = (\hbar k)^2/2m$, the Bogoliubov energy spectrum of the massless (ε_k^+) and massive (ε_k^-) modes are [51, 56, 57]

$$\varepsilon_k^+ = \sqrt{E_k(E_k + 2gn_{\text{1D}})} \quad \varepsilon_k^- = \sqrt{(E_k + 2\hbar J)(E_k + 2\hbar J + 2gn_{\text{1D}})}. \quad (8)$$

If the system is partitioned into the symmetric and antisymmetric fields, as usually done in the literature, there would be no correlation between the two sectors in thermal equilibrium. But our interest lies in the longitudinal cut shown in Fig. 1, where the system is partitioned into gas A and gas B . With this choice, the fields remain correlated at thermal equilibrium as long as $J > 0$. Even without any

tunneling ($J = 0$), correlation can be generated in the initial state by pushing the system far away from equilibrium, e.g., by coherently splitting the system from a single to double-well [14].

2.2. Covariance matrix for Gaussian fields

We characterize the state of the system by the covariance matrix Γ in momentum space, which is a sufficient description for Gaussian fields [58]. To make Γ finite dimensional, infrared (IR) and ultraviolet (UV) cutoffs must be introduced. The IR cutoff is automatically imposed by assuming finite length L and choosing boundary conditions. For the latter, we choose Neumann boundary conditions, consistent with our assumption of an idealized box potential. The UV cutoff is defined by the inverse healing length $\sim \xi_h^{-1}$. We then decompose the fields into summation of discrete modes

$$\hat{\phi}^a(z) = \frac{1}{\sqrt{L}}\hat{\phi}_0^a + \sqrt{\frac{2}{L}} \sum_{k>0}^{k_\Lambda} \hat{\phi}_k^a \cos(kz) \quad (9)$$

$$\delta\hat{n}^a(z) = \frac{1}{\sqrt{L}}\delta\hat{n}_0^a + \sqrt{\frac{2}{L}} \sum_{k>0}^{k_\Lambda} \delta\hat{n}_k^a \cos(kz), \quad (10)$$

where the allowed momenta are $k = N\pi/L$ with $N = 1, 2, 3, \dots, \Lambda$ and the positive integer Λ is chosen such that $k_\Lambda = \Lambda\pi/L \sim \xi_h^{-1}$. The prefactor $\sqrt{2/L}$ ensures proper commutation relation $[\delta\hat{n}_k^a, \hat{\phi}_q^b] = i\delta_{kq}\delta_{ab}$. From here onwards, we consider the case where the zero-mode $\hat{\phi}_0^a, \delta\hat{n}_0^a$ are removed from the data by phase referencing and adjusting for atom number fluctuations.

The covariance matrix $\Gamma \in \mathbb{R}^{4\Lambda \times 4\Lambda}$ is then constructed from the two-point correlation functions of the quadrature operator \hat{Q}^a defined as

$$\hat{Q}^a = \left(\delta\hat{n}_1^a \quad \dots \quad \delta\hat{n}_\Lambda^a \quad \hat{\phi}_1^a \quad \dots \quad \hat{\phi}_\Lambda^a \right)^\top. \quad (11)$$

In our case, it is convenient to organize Γ into a 2×2 block matrix

$$\Gamma = \begin{pmatrix} \Gamma^{AA} & \Gamma^{AB} \\ \Gamma^{BA} & \Gamma^{BB} \end{pmatrix}, \quad (12)$$

where $\Gamma^{ab} \in \mathbb{R}^{2\Lambda \times 2\Lambda}$ are the submatrices with (j, l) element given by

$$\Gamma_{jl}^{ab} = \frac{1}{2} \langle \hat{Q}_j^a \hat{Q}_l^b + \hat{Q}_l^a \hat{Q}_j^b \rangle. \quad (13)$$

The canonical commutation relation imposes the Heisenberg uncertainty principle on physical covariance matrices, i.e.,

$$\Gamma + \frac{i}{2}(\Omega \oplus \Omega) \geq 0, \quad \text{with} \quad \Omega = \begin{pmatrix} 0 & \mathcal{I}_\Lambda \\ -\mathcal{I}_\Lambda & 0 \end{pmatrix} \quad (14)$$

being the symplectic matrix and \mathcal{I}_Λ is the $\Lambda \times \Lambda$ identity matrix. Finally, we remark that in experiments, Γ can be reconstructed from real space phase profiles through a Gaussian tomography scheme [19, 23–25].

2.3. Entanglement measure and mutual information for Gaussian states

The subsystems A and B are correlated as long as $\Gamma^{AB} \neq 0$, which can be due to entanglement or classical correlation. If the state of the joint system is pure, the entanglement entropy (i.e. the von Neumann entropy of the reduced density matrix) quantifies the entanglement. For a Gaussian state, it can be computed through the reduced covariance matrix Γ^{aa} by [19, 30, 58]

$$S(\Gamma^{aa}) = \sum_{q=1}^{\Lambda} \left(\gamma_q^a + \frac{1}{2} \right) \log \left(\gamma_q^a + \frac{1}{2} \right) - \left(\gamma_q^a - \frac{1}{2} \right) \log \left(\gamma_q^a - \frac{1}{2} \right), \quad (15)$$

where γ_q^a are the symplectic eigenvalues of Γ^{aa} , i.e. they are the positive eigenvalues of $i\Omega\Gamma^{aa}$, with $q \in \{1, 2, \dots, \Lambda\}$ labeling the symplectic eigenvalues.

For mixed joint states, entanglement entropy is no longer a valid entanglement measure. Nevertheless, the positive partial transpose (PPT) criterion remains a necessary condition for separability [58]. For continuous variable (CV) systems, partial transposition is equivalent to flipping the sign of the momentum-like fields [59], e.g. in our case $\hat{\phi}_k^B \rightarrow -\hat{\phi}_k^B$ for all modes k . Let us denote the partially transposed covariance matrix as $\Gamma^{\top B}$ and $\gamma_q^{\top B}$ ($q = 1, 2, \dots, 2\Lambda$) as its symplectic eigenvalues. The subsystems A and B are entangled if the logarithmic negativity

$$E_{\mathcal{N}} \equiv \sum_{q=1}^{2\Lambda} \max \{0, -\log (2\gamma_q^{\top B})\} > 0 \quad (16)$$

is positive. When this is true, $E_{\mathcal{N}}$ quantifies the amount of entanglement [60]. The converse is also true for two-mode Gaussian states; if $E_{\mathcal{N}} = 0$, the system is separable

[59, 61]. But in general multimode case, $E_{\mathcal{N}} > 0$ is only a sufficient condition, i.e. there exist bound entangled states with $E_{\mathcal{N}} = 0$ [62].

Another useful measure of correlation is the mutual information $I(A : B)$, which quantifies the total correlations between A and B , including both entanglement and classical correlations. For Gaussian states, it is given by

$$I(A : B) = S(\Gamma^{AA}) + S(\Gamma^{BB}) - S(\Gamma) . \quad (17)$$

The first two terms can be calculated with Eq. (15). For pure joint states, the joint entropy $S(\Gamma) = 0$, and so the mutual information is precisely twice the entanglement entropy. For mixed joint states, $S(\Gamma)$ does not vanish in general, but it is computable through Eq. (15) with the symplectic matrix being $\Omega \oplus \Omega$ and q runs until 2Λ . Logarithmic negativity and mutual information are the two correlation measures we will focus on in this paper.

3. Results: Entanglement and mutual information at finite temperatures

In tunnel-coupled Luttinger liquids, the low-energy Hamiltonian separates into symmetric (+) and antisymmetric sectors (-). The system is thus described by a two-species bosonic theory comprising a massless symmetric mode and a massive antisymmetric mode. Assuming Neumann boundary conditions, we use Bogoliubov transformation [18, 51, 56, 57] to expand the phase and density fluctuations in terms of bosonic creation and annihilation operators \hat{b}_k^\pm in the two sectors

$$\hat{\phi}_k^+ = \frac{1}{\sqrt{4n_{1D}}} \sqrt{\frac{\varepsilon_k^+}{E_k}} [\hat{b}_k^+ + \text{h.c.}] \quad \delta\hat{n}_k^+ = \sqrt{n_{1D}} \sqrt{\frac{E_k}{\varepsilon_k^+}} [i\hat{b}_k^+ + \text{h.c.}] \quad (18)$$

$$\hat{\phi}_k^- = \frac{1}{\sqrt{4n_{1D}}} \sqrt{\frac{\varepsilon_k^-}{E_k + 2\hbar J}} [\hat{b}_k^- + \text{h.c.}] \quad \delta\hat{n}_k^- = \sqrt{n_{1D}} \sqrt{\frac{E_k + 2\hbar J}{\varepsilon_k^-}} [i\hat{b}_k^- + \text{h.c.}] , \quad (19)$$

where $E_k = (\hbar k)^2/(2m)$ is the free particle dispersion, ε_k^\pm are the Bogoliubov energy spectra defined in Eq. (8).

In this section, we will assume the system is at thermal equilibrium, having a density matrix $\rho \propto \exp(-\beta\hat{H})$ with inverse temperature β . The elements of the covariance matrix Γ^{ab} can be calculated from Eqs. (18) and (19). For example, the

phase-phase correlations are

$$\langle \hat{\phi}_k^a \hat{\phi}_q^b \rangle = \begin{cases} \frac{1}{2} \left(\langle \hat{\phi}_k^+ \hat{\phi}_k^+ \rangle + \langle \hat{\phi}_k^- \hat{\phi}_k^- \rangle \right) \delta_{kq} & \text{if } a = b \\ \frac{1}{2} \left(\langle \hat{\phi}_k^+ \hat{\phi}_k^+ \rangle - \langle \hat{\phi}_k^- \hat{\phi}_k^- \rangle \right) \delta_{kq} & \text{if } a \neq b, \end{cases} \quad (20)$$

and a similar equation also holds for the density-density correlations, while the phase-density correlations vanish in equilibrium.

Crucially, all correlation functions vanish for different momentum modes $k \neq q$, implying that the k -mode of gas A can only be correlated with the same k -mode of gas B . Characterizing entanglement thus reduces to solving a series of independent two-mode entanglement problem, for which PPT criterion is necessary and sufficient [59, 61]. Another important consequence is that the entanglement and mutual information are monotone under adding and removing any mode k . Hence, we can justifiably ignore the contribution from the zero mode ($k = 0$) and the modes above the UV cutoff ($k > k_\Lambda$). The calculated logarithmic negativity and mutual information by ignoring these modes can be treated as lower bound for the true logarithmic negativity and mutual information of the system.

The transformation from A, B to \pm basis diagonalizes the covariance matrix while preserving the symplectic eigenvalues (see Appendix A). This allows for analytic evaluation of the symplectic eigenvalues, and consequently also the logarithmic negativity and the mutual information. We begin by presenting our result for the logarithmic negativity

$$E_{\mathcal{N}} = \sum_{k>0}^{k_\Lambda} \max \left\{ 0, -\log \left[\sqrt{\frac{\varepsilon_k^-}{\varepsilon_k^+} \frac{E_k}{E_k + 2\hbar J} (1 + 2\eta_k^+) (1 + 2\eta_k^-)} \right] \right\}, \quad (21)$$

where

$$\eta_k^\pm = \langle (\hat{b}_k^\pm)^\dagger \hat{b}_k^\pm \rangle = [\exp(\beta \varepsilon_k^\pm) - 1]^{-1} \quad (22)$$

are the mean thermal occupations in the symmetric and antisymmetric sectors. The result can be generalized to the case where each sector has a different temperature ($\beta^+ \neq \beta^-$) by appropriately defining η_k^\pm . From Eq. (21), we see a competition between tunneling strength J and the temperature $T = (k_B \beta)^{-1}$ in establishing entanglement (k_B is the Boltzmann constant). On the one hand, tunneling tends to create entanglement since the spectral ratio satisfies $(\varepsilon_k^- / \varepsilon_k^+) (E_k / (E_k + 2\hbar J)) \leq 1$ with the inequality being saturated at $J = 0$. On the other hand, temperature tends to destroy entanglement with the term $(1 + 2\eta_k^+) (1 + 2\eta_k^-) \geq 1$.

For a fixed tunneling strength, we calculate the threshold temperature T^* above which entanglement vanishes, i.e. $E_{\mathcal{N}}(T) = 0$ for all $T > T^*$ where

$$T^* = \sup_{0 < k \leq k_{\Lambda}} \left\{ T_k^* \left| \tanh \left(\frac{\varepsilon_k^+}{2k_B T_k^*} \right) \tanh \left(\frac{\varepsilon_k^-}{2k_B T_k^*} \right) = \frac{\varepsilon_k^-}{\varepsilon_k^+} \frac{E_k}{E_k + 2\hbar J} \right\}, \quad (23)$$

easily solvable by root-finding. Applying this formula reveals that the threshold temperature increases with stronger tunneling (Fig. 2a). Similarly, one may fix the temperature and find the critical tunneling strength needed to observe entanglement, which would be stronger for higher temperatures.

At this point, we remark that while the Hamiltonian (6) can be written as coupled quantum harmonic oscillators, whose thermal entanglement and threshold temperature have been studied in a general setting [7, 8], we identify a solvable and experimentally relevant instance of such models. We also go further by evaluating the experimental attainability of the threshold temperature and exploring the entanglement scaling with tunable system parameters such as tunneling strength, system's length, and mean density. Later in the section, we will probe the transition point between quantum and classical correlation by comparing logarithmic negativity with mutual information.

We plot a phase diagram for entanglement as measured by $E_{\mathcal{N}}$ with varying temperature T and tunneling strength J in Fig. 2a. We identify the parameter regimes where the system is entangled ($E_{\mathcal{N}} > 0$) and where it is separable ($E_{\mathcal{N}} = 0$), separated by the threshold temperature T^* curve. In the entangled regime, entanglement intuitively increases with stronger tunneling and decreases with increasing temperature. For the experimental parameters used in Refs. [18, 19, 25], T^* lies in the range of $1 \sim 5$ nK, about one order of magnitude lower than the temperatures achieved in these experiments.

Given a fixed tunneling strength, the largest T_k^* typically occurs for the largest accessible mode k_{Λ} . We interpret this as the entanglement in higher momentum modes being more robust to thermal noise. As one raises the temperature, thermal noise corrupts the entanglement in all modes, but it corrupts the entanglement in low momentum modes more quickly. For instance, above the first threshold $T > T_{k_1}^*$ ($k_1 = \pi/L$), the entanglement between A and B vanishes for k_1 , while still possibly present for $k > k_1$ (Fig. 2b). This process continues until all entanglement in the modes $k \leq k_{\Lambda}$ vanishes at $T = T^*$ and we no longer observe entanglement. Naturally, the ability to detect entanglement depends on the cutoff Λ . For a fixed

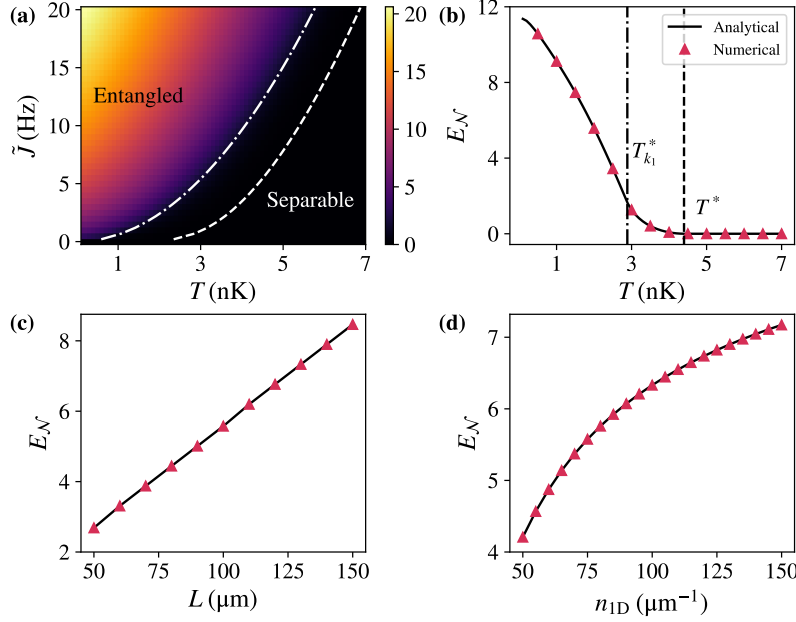


Figure 2. *Entanglement at finite temperatures for tunnel-coupled gases.*— (a) Entanglement phase diagram with respect to tunneling strength $\tilde{J} = J/(2\pi)$ and temperature T as measured by logarithmic negativity $E_{\mathcal{N}}$. The dashed line is the threshold temperature T^* above which entanglement vanishes ($E_{\mathcal{N}} = 0$) for all modes $k \leq k_{\Lambda}$. The dashed-dotted line is the first threshold temperature $T_{k_1}^*$ above which the entanglement in the first mode $k_1 = \pi/L$ vanishes, while still possibly present in higher momentum modes with $k > k_1$. (b) The decay of $E_{\mathcal{N}}$ with increasing T for fixed tunneling $\tilde{J} = 5$ Hz. For panels (b)-(d), the solid lines are calculated with our analytical formula (21), while the triangles are numerically computed with numerical diagonalization. The dashed and dashed-dotted lines have the same meaning as in (a). (c) Linear scaling of $E_{\mathcal{N}} \propto L$ for fixed temperature $T = 2$ nK and fixed tunneling strength $\tilde{J} = 5$ Hz. The cutoff Λ changes for different L since we set $k_{\Lambda} = \Lambda\pi/L \sim \xi_h^{-1}$. In panels (a) - (c), mean density is fixed at $n_{1D} = 75 \mu\text{m}^{-1}$, but the results do not significantly change for other n_{1D} values. (d) Sub-linear scaling of $E_{\mathcal{N}}$ with mean density n_{1D} . The difference between scaling behavior in (c) and (d) underscores the collective nature of 1D excitations. For panels (a), (b), and (d), the condensate length is fixed at $L = 100 \mu\text{m}$. The mass m is the atomic mass ^{87}Rb . The interaction strength g is close to the value reported in the experiments (see e.g. Refs. [19, 25] among others) and fixed throughout the paper, i.e. $g \approx 2\hbar a_s \omega_{\perp}$ where $a_s \approx 5.2$ nm is the scattering length, and $\omega_{\perp} = 2\pi \times 2$ kHz is the transverse trapping frequency.

cutoff $k_\Lambda \sim \xi_h^{-1}$ the system can be regarded as ‘effectively separable’ at $T > T^*$, even though entanglement may still persist above the cutoff. Conversely, the experimental imaging resolution is typically lower than ξ_h^{-1} , and so depending on the specific resolution, the threshold temperature in experiments can be lower than in Fig. 2.

We next investigate the scaling of entanglement with the subsystem’s length L . Previous theoretical work [47, 48] has shown that in the ground state, entanglement behaves extensively, meaning it grows linearly with L . We obtain the same result for finite temperature states as long as the temperature is sufficiently far away from T^* as shown in Fig. 2c. We next provide a simple argument to explain this. Given a fixed resolution, the number of allowed k -modes increases linearly with L , i.e. in the continuum limit $\sum_k \rightarrow (L/2\pi) \int dk$. In our setting, this is the dominant mechanism by which entanglement grows with length $E_{\mathcal{N}} \propto L$. We emphasize that this extensivity arises due to the embedding of the 1D systems in 2D space, so it does not violate the standard area law for a strictly 1D system. Interestingly, the scaling behavior is sublinear if we increase mean density n_{1D} instead of L (Fig. 2d), underscoring the collective nature of excitations, as entanglement does not just scale linearly with atom number $n_{1D}L$.

Above the threshold temperature $T > T^*$, A and B are effectively separable but they can still be classically correlated. We probe the transition from quantum to classical correlation by calculating the mutual information (see Appendix A for derivation)

$$I(A : B) = \sum_{k>0}^{k_\Lambda} 2 \left[\left(\lambda_k + \frac{1}{2} \right) \log \left(\lambda_k + \frac{1}{2} \right) - \left(\lambda_k - \frac{1}{2} \right) \log \left(\lambda_k - \frac{1}{2} \right) \right] \\ - \sum_{a=\pm} \sum_{k>0}^{k_\Lambda} [(\eta_k^a + 1) \log (\eta_k^a + 1) - \eta_k^a \log \eta_k^a], \quad (24)$$

where λ_k are the symplectic eigenvalues of the reduced covariance matrix, which are given by

$$\lambda_k = \frac{1}{4} \sqrt{[(1 + 2\eta_k^+) + C_k(1 + 2\eta_k^-)] [(1 + 2\eta_k^+) + C_k^{-1}(1 + 2\eta_k^-)]} \quad (25)$$

and $C_k = (\varepsilon_k^- / \varepsilon_k^+) (E_k / (E_k + 2\hbar J))$ is the spectral ratio also appears in the expression for $E_{\mathcal{N}}$ in Eq. (21).

In Fig. 3a we probe the behavior of mutual information $I(A : B)$ in the vicinity of the threshold temperature T^* . In contrast to decaying entanglement,

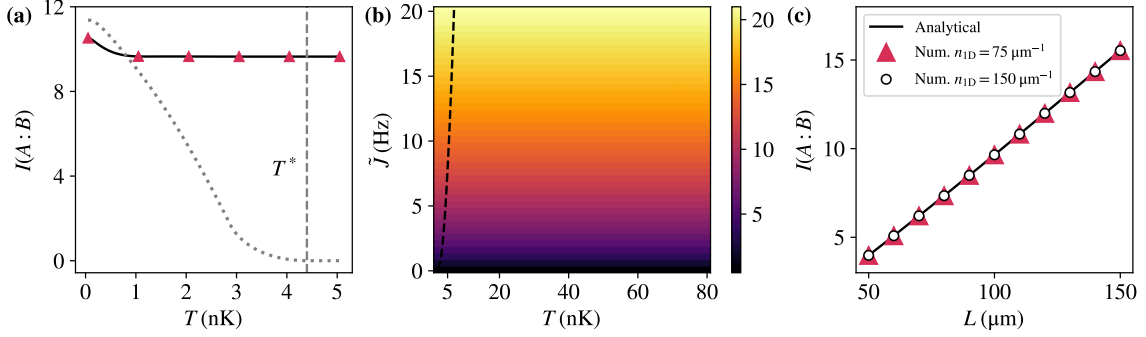


Figure 3. *Mutual information at finite temperatures for tunnel-coupled gases.*— (a) Crossover from quantum to classical correlations near the threshold temperature T^* (dashed line). The mutual information $I(A : B)$ (solid line) is constant while the logarithmic negativity $E_{\mathcal{N}}$ (dotted) line decays to zero. The tunneling strength is fixed at $\tilde{J} = J/(2\pi) = 5$ Hz. (b) $I(A : B)$ tend to increase with stronger J but it is almost constant with T , even way above T^* (black dashed line). For panels (a) and (b), the condensate length is fixed at $L = 100 \mu\text{m}$. (c) Linear scaling of mutual information with system's length $I(A : B) \propto L$ for fixed temperature $T = 30$ nK and fixed tunneling strength $\tilde{J} = 5$ Hz. For panels (a) and (c), the solid line is calculated with Eq. (24) while the triangles and the circles are calculated with numerical diagonalization. The mean density is fixed at $n_{1D} = 75 \mu\text{m}^{-1}$ in all panels except for the circles in panel (c) where $n_{1D} = 150 \mu\text{m}^{-1}$, indicating that mutual information does not significantly scale with n_{1D} .

$I(A : B)$ stays approximately constant. Meanwhile, the magnitude of $I(A : B)$ is comparable to $E_{\mathcal{N}}$ below T^* , meaning that below the threshold, a significant portion of the correlation consists of quantum entanglement. As one approaches T^* , the entanglement must get transformed into classical correlations to keep the mutual information constant.

The approximate independence of mutual information with respect to temperature persists far above T^* as shown in Fig. 3b. Intuitively, this can be explained if the role of temperature is only to rescale the magnitude of the local fluctuations in A and B without affecting their shared information. Instead, the shared information is governed by the tunneling strength, as supported by $I(A : B)$ monotonically increasing with stronger tunneling. Finally, for the same reason as the entanglement, the mutual information also scales linearly with the subsystem's length $I(A : B) \propto L$ (Fig. 3c). But unlike entanglement, our analytical and numerical

results show that the mutual information does not significantly scale with mean density.

So far, the correlation between the subsystems A and B is induced by tunnel-coupling at the Hamiltonian level and investigated in thermal equilibrium. In the context of experiments in Refs. [11, 12, 17–19], the temperature needed to observe entanglement between the two gases is an order of magnitude lower than what has been experimentally demonstrated. In the next section, we explore another scenario where the threshold temperature to observe entanglement is within experimental reach. The scenario involves pushing the system far away from equilibrium by coherent splitting.

4. Results: Entanglement and mutual information after coherent splitting

In the coherent splitting scenario, the system is assumed to be initialized in thermal equilibrium of a single well at $t < 0$. Then, the single-well potential is coherently split into a double-well at $t = 0$ within a timescale much shorter than the interaction timescale ($\Delta t_{\text{split}} \ll \xi_h/c$ with $c = \sqrt{gn_{1D}/m}$ being the speed of sound), such that its effect is analogous to an ideal beam splitter. Let \hat{b}^0 be the phonon annihilation operator before the splitting, and $\hat{b}^{A,B}$ be the phonon annihilation operators after the splitting, respectively. The case of coherent splitting is analogous to an equal beam splitter with one input being \hat{b}^0 , occupied by a thermal state, and the other input being an ancilla \hat{b}^{anc} , occupied by a vacuum. At the output (i.e. after the splitting), all the initial thermal energy gets transferred to the symmetric sector due to the beam splitter operation $\hat{b}^+ = (\hat{b}^A + \hat{b}^B)/\sqrt{2} = \hat{b}^0$. On the other hand, the antisymmetric mode $\hat{b}^- = (\hat{b}^A - \hat{b}^B)/\sqrt{2} = \hat{b}^{\text{anc}}$ has a minimum uncertainty as it is occupied by the vacuum of the ancilla. If we also reasonably assume \hat{b}^0 and \hat{b}^{anc} are initially uncorrelated, it follows that \hat{b}^+ and \hat{b}^- are uncorrelated at the output.

Meanwhile, locally, the atoms undergo a random process of going either to the left or right well, giving excess noise to the relative density $\delta\hat{n}^-$ while squeezing the relative phase $\hat{\phi}^-$. Phenomenologically, the correlation in the antisymmetric sector after the instantaneous splitting is modelled as a squeezed vacuum of the form [17, 63, 64]

$$\langle \hat{\phi}_k^- \hat{\phi}_q^- \rangle \Big|_{t=0} = \frac{1}{2n_{1D}} \frac{\delta_{kq}}{r^2} \quad \langle \delta\hat{n}_k^- \delta\hat{n}_q^- \rangle \Big|_{t=0} = \frac{n_{1D}}{2} \delta_{kq} r^2, \quad (26)$$

while the phase-density correlations vanish (see e.g. Refs [64, 65] for more theoretically systematic derivations). Here, r is the squeezing parameter, introduced to take into account fluctuation due to technical noise from finite-time splitting [32, 66, 67], or squeezing enhancement accessible in recent experiments [36, 37]. Following the beam splitter argument, the symmetric fluctuation is modelled as thermal with a temperature equal to the condensate before the splitting, and uncorrelated with those in the antisymmetric sector. We remark that although there have been many experimental works on relaxation after coherent splitting, the precise control and characterization of the initial state is a subject of ongoing research [22, 65, 68].

In Subsec. 4.1 we will study the logarithmic negativity and the mutual information immediately after the coherent splitting ($t = 0$). Then, in Subsec. 4.2, we discuss how the conservation of mutual information constrains relaxation toward a prethermalized state ($t > 0$) [17, 33, 63].

4.1. Initial entanglement and mutual information at $t = 0$

For the initial non-equilibrium state after coherent splitting, the symmetric and antisymmetric sectors are separated and there is no correlation between modes with different momenta. These features also appear in the equilibrium tunnel-coupled case (Sec. 3), allowing us to analytically calculate the logarithmic negativity and the mutual information. We thus extend the calculation done in Sec. 3 to this non-equilibrium state. The details of the calculation is given in Appendix B. Here, we present the expression for logarithmic negativity

$$E_{\mathcal{N}} = \sum_{k>0}^{k_{\Lambda}} \max \left\{ 0, -\log \left[\frac{2}{r} \sqrt{\frac{E_k}{\varepsilon_k^+} \left(\eta_k^+ + \frac{1}{2} \right)} \right] \right\} + \max \left\{ 0, -\log \left[r \sqrt{\frac{\varepsilon_k^+}{E_k} \left(\eta_k^+ + \frac{1}{2} \right)} \right] \right\}. \quad (27)$$

From Eq. (27), we see again a competing behavior: squeezing r and the interaction energy gn_{1D} (appearing through ε_k^+) generate entanglement, while temperature appearing through η_k^+ suppresses it. For squeezing parameters $r \geq 1$, the first term dominates, whereas for $r \ll 1$, the second term may dominate.

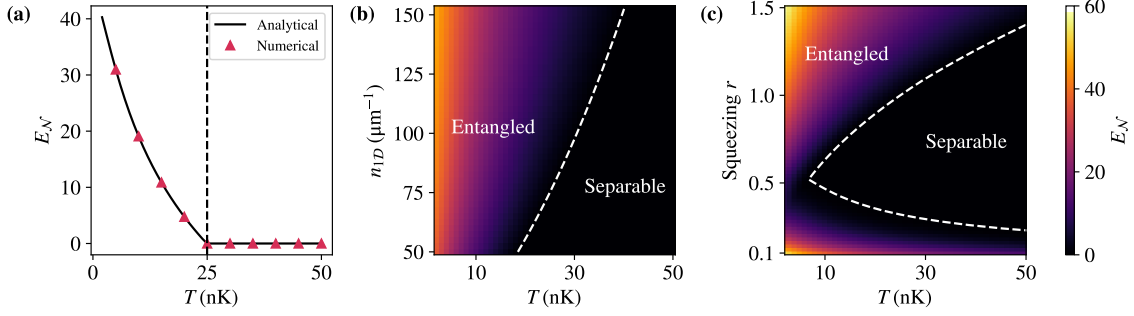


Figure 4. *Entanglement immediately after coherent splitting.*— (a) Logarithmic negativity E_N as a function of temperature T for $r = 1$ and $n_{1D} = 75 \mu\text{m}^{-1}$. All dashed lines indicate the threshold temperature T^* . For parameters in panel (a) the threshold temperature is calculated to be $T^* \approx 25$ nK. The solid line is calculated with Eq. (27) and the triangles are computed with numerical diagonalization. Entanglement phase diagram as a function of temperature and (b) mean density n_{1D} (fixed $r = 1$), and (c) squeezing parameter $0.1 \leq r \leq 1.5$ (fixed $n_{1D} = 75 \mu\text{m}^{-1}$). The obtained range for T^* is accessible in the present day experiments [19, 32]. Both E_N and T^* behave non-monotonically with r . The condensate length is fixed at $L = 100 \mu\text{m}$ for all panels. The condensate length is fixed at $L = 100 \mu\text{m}$, while further numerics show that logarithmic negativity still scales linearly with length $E_N \propto L$, as long as the temperature is sufficiently far away from the threshold temperature.

Surprisingly, the threshold temperature T^* can be expressed in a closed form

$$T^* = \sup_{0 < k \leq k_\Lambda} \left\{ T_k^* = \frac{\varepsilon_k^+}{k_B} \left(\ln \sqrt{\frac{F(k, r)}{F(k, r) - 2}} \right)^{-1} \right\} \quad F(k, r) \equiv 1 + \frac{r^2 \varepsilon_k^+}{4 E_k} + \frac{1}{r^2} \frac{E_k}{\varepsilon_k^+}. \quad (28)$$

Note that when $F(k, r) \leq 2$, T_k^* has no real solution, meaning for the associated mode k , no entanglement is generated at any temperature. This regime occurs when the squeezing parameter $r \sim 1$ and $\varepsilon_k^+/E_k \sim 1$. The latter corresponds to quasiparticle excitations behaving as free particle instead of phonons, which happens in high momenta where the spectrum's curvature becomes important [69, 70]. Thus, for squeezing $r \sim 1$, entanglement is mainly generated in the low-momentum modes.

In Fig. 4, we plot E_N and T^* for realistic experimental parameters. We first focus on fixed squeezing $r = 1$ and mean density $n_{1D} = 75 \mu\text{m}^{-1}$ (Fig. 4a) and

calculate the threshold temperature to be $T^* \approx 25$ nK. The threshold temperature can be raised further by increasing interaction energy gn_{1D} (Fig. 4b) or by increasing squeezing parameter r (Fig. 4c). For realistic range of experimental parameters, T^* is found to be between $20 \sim 40$ nK, which is readily accessible in the present day experiments [19, 32].

Moreover, we find that both $E_{\mathcal{N}}$ and T^* behave non-monotonically with the squeezing parameter r (Fig. 4c). The system exhibits entanglement for both large ($r > 1$) and small ($r < 0.2$) squeezing, but the entanglement and the regime of entanglement are strongly suppressed at intermediate squeezing values ($0.2 < r < 1$). This can be understood from the initial correlation in Eq. (26). As the source of the entanglement is the initial squeezing in the relative phase, setting $r > 1$ ($r < 1$) would enhance (suppress) the squeezing and thus increase (decrease) the entanglement. But crucially, when r is very small (e.g. $r < 0.2$), we are in the opposite regime wherein the density fluctuation is squeezed and so entanglement re-emerge through the second term in Eq. (27).

To gain more insight into the crossover between quantum and classical correlations after coherent splitting, we compute the mutual information

$$I(A : B) = 2 \sum_{k>0}^{k_{\Lambda}} \left[\left(\lambda_k + \frac{1}{2} \right) \log \left(\lambda_k + \frac{1}{2} \right) - \left(\lambda_k - \frac{1}{2} \right) \log \left(\lambda_k - \frac{1}{2} \right) \right] - (1 + \eta_k^+) \log(1 + \eta_k^+) + \eta_k^+ \log \eta_k^+, \quad (29)$$

where

$$\lambda_k = \frac{1}{4} \sqrt{(1 + 2\eta_k^+ + \mathcal{C}_k)(1 + 2\eta_k^+ + \mathcal{C}_k^{-1})} \quad (30)$$

and $\mathcal{C}_k = (r^2/2)(\varepsilon_k^+/E_k)$. Note that the λ_k above has a similar form as that of Eq. (25) since in both scenarios the covariance matrices have the same structure, differing only in the matrix elements in the antisymmetric sector.

In Fig. 5a, we plot $I(A : B)$ as a function of temperature T for fixed squeezing $r = 1$ and fixed mean density $n_{1D} = 75 \mu\text{m}^{-1}$. Contrary to the decay of entanglement (Fig. 4a), mutual information grows with temperature irrespective of the threshold. We interpret this as the system being driven further from equilibrium with increasing temperature as the difference between the symmetric and antisymmetric modes becomes more pronounced. This results in a build-up of classical correlations that must not only be enough to compensate for the decaying quantum correlations, but

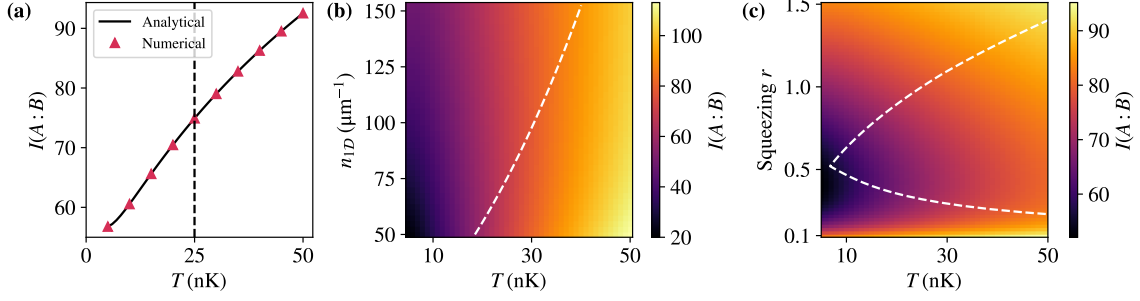


Figure 5. *Mutual information immediately after coherent splitting.*— (a) The increase of mutual information $I(A : B)$ with increasing temperature T for fixed squeezing $r = 1$ and mean density $n_{1D} = 75 \mu\text{m}^{-1}$, in contrast with decaying $E_{\mathcal{N}}$ in Fig. 4a. The solid line is calculated with Eq. (29) and the triangles are computed with numerical diagonalization. (b) The mutual information $I(A : B)$ varies slowly with mean density n_{1D} . Here the squeezing is fixed at $r = 1$. (c) Similar to entanglement, $I(A : B)$ also changes non-monotonically with squeezing parameter r ($n_{1D} = 75 \mu\text{m}^{-1}$). In all panels, the dashed lines represent the threshold temperature T^* , same as in Fig. 4. The condensate length is fixed at $L = 100 \mu\text{m}$, while further numerics show that mutual information still scales linearly with length $I(A : B) \propto L$.

must also add to the overall correlations. This trend does not significantly change as we vary the mean density (Fig. 5b). Similar to entanglement, $I(A : B)$ is also found to behave non-monotonically with squeezing parameter. In Fig. 5c, we observe that $I(A : B)$ is strongly suppressed at low temperatures ($T < 20$ nK) and intermediate squeezing regime ($0.2 < r < 1$) where entanglement is also suppressed (Fig. 4c).

4.2. Relaxation constrained by mutual information conservation

In experiments [17, 33], the double-well barrier after coherent splitting is set to be high enough such that no tunneling is allowed between the two gases A and B . Consequently, the system's dynamics follows that of decoupled TLL [Eq. (4) with $J = 0$], i.e. $\hat{H} = \hat{H}_{\text{TLL}}^+ + \hat{H}_{\text{TLL}}^-$. Interestingly, the relative phase fluctuation $\hat{\phi}^-(z)$ is experimentally observed to relax into a thermal-like metastable state with an effective inverse temperature $\beta^- = (gn_{1D}/2)^{-1}$, independent of the system's initial temperature before the splitting [17, 34, 35]. The temperature in the relative sector is inferred from the measured relative phase correlation functions

and its full distribution functions [15, 17, 35, 71], whose behavior is found to be consistent with thermal ensemble after relaxation. This phenomenon is an example of prethermalization, widespread in out-of-equilibrium integrable systems [72, 73]. The prethermalization in these experiments arises from the multimode dephasing due to coherent rotation between the relative density and the relative phase fluctuations [17, 24, 32].

Here, we argue that local unitary dynamics generated by decoupled TLL *cannot* bring the coherently split initial state [Eq. (26)] to a Generalized Gibbs ensemble (GGE) [34, 74] of the form

$$\rho_{\text{GGE}} = \frac{1}{Z} \exp(-\beta^- \hat{H}_{\text{TLL}}^-) \otimes \exp(-\beta^+ \hat{H}_{\text{TLL}}^+) , \quad (31)$$

which is sometimes conjectured to be the relaxed prethermalized state in the past experimental and numerical studies [17, 34, 75], at least approximately. The reason is that the Hamiltonian governing the dynamics is not only decoupled in the \pm basis, but it is also decoupled in A, B basis: $\hat{H} = \hat{H}_{\text{TLL}}^A + \hat{H}_{\text{TLL}}^B$. Consequently, the unitary dynamics generated by \hat{H} must conserve the mutual information (and in general, also entanglement) between subsystem A and subsystem B , i.e., $I(A : B, t) = I(A : B, 0)$ for all $t > 0$.

Meanwhile, we can compute the mutual information for GGE states of the form (31) as a special case of Eq. (24) with $J = 0$ and $\beta^+ \neq \beta^-$. We obtain

$$\begin{aligned} I_{\text{GGE}}(A : B) &= \sum_{k>0}^{k_\Lambda} 2 [(1 + \bar{\eta}_k) \log(1 + \bar{\eta}_k) - \bar{\eta}_k \log \bar{\eta}_k] \\ &\quad - \sum_{a=\pm} \sum_{k>0}^{k_\Lambda} [(\eta_k^a + 1) \log(\eta_k^a + 1) - \eta_k^a \log \eta_k^a] , \end{aligned} \quad (32)$$

where $\bar{\eta}_k = \frac{1}{2}(\eta_k^+ + \eta_k^-)$ is the average of mean thermal occupations in both sectors. By comparing Eq. (32) with Eq. (29), one finds that mutual information is not conserved, hence a contradiction.

Indeed, a detailed theoretical analysis on the relaxation of correlation functions, including the density-density and phase-density correlations, starting from coherently split initial state and following TLL dynamics has been done [64]. It was revealed that the relaxed state is not compatible with a thermal equilibrium, despite some correlation functions agreeing with thermal behavior. Our result highlights another

physical constraint, the mutual information conservation, in the subtle process of relaxation and prethermalization of isolated 1D quantum gases.

Alternatively, the system could still prethermalize into GGE of the form (31) in experiments, but it does that not by evolving according to the TLL model. The TLL model is only effective and the exact model almost certainly features non-zero interactions, although the time-scale at which interaction becomes relevant is unclear [18, 76–78]. In the long-time limit, the system is expected to thermalize at phonon-levels into a thermal state with $\beta^+ = \beta^- = \beta$, having zero mutual information $I(A : B) = 0$ for decoupled double-well ($J = 0$). This process is expected to occur via anharmonic correction to TLL which include three-body phonon interaction [75, 76, 79–81]. Experimentally, the physics beyond TLL has not been probed due to the lack of access to the relevant observables [77, 80]. This can now potentially be solved by using common phase measurement [38], giving ways to more detailed and rigorous tests to the GGE hypothesis.

Introducing phonon-phonon interaction into the effective model can lead to interesting dynamics for the entanglement and mutual information studied here. This is because the evolution become effectively non-unitary as excitations may leak to momentum states above the cutoff and to the non-Gaussian degrees of freedom. In experiments, the spatial resolution of the measurements places a cut-off on the momenta that can be resolved [53, 54]. A universal flow of momentum excitations has previously been argued [82]. This means that the dynamics will appear to ‘move’ certain excitations out of view while also ‘move’ some excitations into view. Moreover, interaction may lead to non-Gaussian correlations, whose presence implies that the entropic quantities evaluated under the assumption of the state being Gaussian may not be accurate. However, as long as the non-Gaussian state does not depart too far from being Gaussian, the entropy is continuous under the assumption of a finite energy [83]. If ρ is an arbitrary state, there exists a unique Gaussian state ρ_G with the same second moments Γ as ρ . The entropy computed using the Gaussian formula for ρ_G will overestimate the true entropy of ρ , i.e. $S(\rho) \leq S(\rho_G)$. This is because Gaussian entropy disregards higher-order correlations as if they were unobserved, which for a non-Gaussian state corresponds to a lack of knowledge reflected in the higher entropy value. How exactly these momentum cutoff and non-Gaussian correlations affect entanglement and mutual information during relaxation dynamics is a subject for further research.

5. Summary and Outlook

We have studied entanglement and mutual information between coupled Tomonaga-Luttinger liquids partitioned along the longitudinal axis at finite temperatures and after coherent splitting. We unambiguously established that the entanglement and mutual information across this partition are extensive, by showing that both quantities scale linearly with the subsystem length. Importantly, we also identified the threshold temperature for observing entanglement, and found that in the case of coherent splitting, the temperature range is already within experimental reach.

Our study explores the dependence of entanglement and mutual information on key physical parameters, including temperature, tunneling strength, mean density, and the squeezing parameter. Our results suggest that mutual information—a key correlation measure employed in previous experiments [19, 25]—often reflects classical correlations and therefore cannot reliably capture the entanglement features of the system in the scenarios considered here. Nevertheless, it provides us with other important insights, including the quantum-to-classical correlation transition near the threshold temperature, and the conservation of mutual information in the non-interacting TLL dynamics, which forbids prethermalization to GGE states with distinct temperatures in the symmetric and antisymmetric sectors, unless phonon-phonon interaction is taken into account.

A strong motivation for this work is the goal to experimentally detect extensive entanglement in many-body quantum systems. Our results suggest that such detection is not only feasible in 1D Bose gas experiments, but the required measurement protocol is also accessible. Specifically, one may apply the existing Gaussian tomography [23, 24] in both antisymmetric and symmetric sectors to reconstruct the full covariance matrix. This is made possible by recent developments in matter-wave interferometry after time-of-flight, allowing for single-shot extraction of not only relative but also common phase fluctuations [38]. Thus, while many studies on entanglement in field theories remain largely theoretical, this work highlights a clear pathway that could be pursued experimentally.

On the other hand, experimental detection of entanglement brings about other challenges that have not been addressed here. For instance, certifying the reliability of Gaussian tomography reconstruction for witnessing entanglement includes taking into account statistical fluctuations, inherent systematic error in the phases extraction protocols [38, 54], and imperfections in the imaging which

are known to introduce convolutions to the measured density interference patterns [23, 52]. Furthermore, typical experiments involve harmonic trapping, meaning that the system deviates from being fully homogeneous. In such situations, correlations between different momentum modes could become non-negligible, implying that logarithmic negativity is no longer a necessary and sufficient entanglement witness, and that the zero modes and the modes above the UV cutoff might affect the overall correlation. Even in experiments with a box potential [12, 18, 19, 21], the mean density curvature due to imperfect box should be scrutinized. A numerical and experimental study on precise certification of entanglement and mutual information from density interference data is an important direction for future work.

Another direction of interest to both theory and experiment is to consider relaxation dynamics of entanglement and mutual information after a sudden quench (e.g. coherent splitting) or in the presence of a generic time-dependent tunneling strength. One may theoretically study these problems in the limit of low-energy theories—the Tomonaga-Luttinger liquid and the sine-Gordon model—or probe deviations from low energy theories and investigate the impact of cutoff and non-Gaussian correlations as discussed in the previous section. The latter is more challenging theoretically but it is highly relevant for experiments. Equipped with reliable Gaussian tomography, the long-time relaxation of Gaussian entanglement and mutual information can in principle be probed experimentally [77].

The presented work thus contributes to ongoing efforts in both theory and experiment for exploring entanglement in low-dimensional strongly correlated quantum matter, both in and out of equilibrium. By providing a timely theoretical foundation, this work paves the way for rigorous quantum simulation of interacting quantum field theories in cold-atomic platforms.

6. Acknowledgements

We are grateful to Jörg Schmiedmayer and Léonce Dupays for their valuable feedback. We also thank Paola Ruggiero, Julia Mathé, Nicky Kai Hong Li, and Giuseppe Vitagliano for insightful discussions. This work was supported by the start-up grant of the Nanyang Assistant Professorship of Nanyang Technological University, Singapore.

References

- [1] John S Bell. “On the Einstein-Podolsky-Rosen Paradox”. *Physics Physique Fizika* **1**, 195 (1964).
- [2] Ryszard Horodecki, Paweł Horodecki, Michał Horodecki, and Karol Horodecki. “Quantum entanglement”. *Rev. Mod. Phys.* **81**, 865–942 (2009).
- [3] Nicolai Friis, Oliver Marty, Christine Maier, Cornelius Hempel, Milan Holzäpfel, Petar Jurcevic, Martin B. Plenio, Marcus Huber, Christian Roos, Rainer Blatt, and Ben Lanyon. “Observation of entangled states of a fully controlled 20-qubit system”. *Phys. Rev. X* **8**, 021012 (2018).
- [4] Nicolai Friis, Giuseppe Vitagliano, Mehul Malik, and Marcus Huber. “Entanglement certification from theory to experiment”. *Nat. Rev. Phys.* **1**, 72–87 (2019).
- [5] Sadegh Raeisi, Pavel Sekatski, and Christoph Simon. “Coarse graining makes it hard to see micro-macro entanglement”. *Phys. Rev. Lett.* **107**, 250401 (2011).
- [6] Tian Wang, Roohollah Ghobadi, Sadegh Raeisi, and Christoph Simon. “Precision requirements for observing macroscopic quantum effects”. *Phys. Rev. A* **88**, 062114 (2013).
- [7] Janet Anders. “Thermal state entanglement in harmonic lattices”. *Phys. Rev. A* **77**, 062102 (2008).
- [8] Janet Anders and Andreas Winter. “Entanglement and separability of quantum harmonic oscillator systems at finite temperature”. *Quantum Inf. Comput.* **8**, 245–262 (2008).
- [9] Thierry Giamarchi. “Quantum Physics in One Dimension”. Oxford University Press. (2003).
- [10] Vladimir Gritsev, Anatoli Polkovnikov, and Eugene Demler. “Linear response theory for a pair of coupled one-dimensional condensates of interacting atoms”. *Phys. Rev. B* **75**, 174511 (2007).
- [11] Thomas Schweigler, Valentin Kasper, Sebastian Erne, Igor Mazets, Bernhard Rauer, Federica Cataldini, Tim Langen, Thomas Gasenzer, Jürgen Berges, and Jörg Schmiedmayer. “Experimental characterization of a quantum many-body system via higher-order correlations”. *Nature* **545**, 323–326 (2017).

- [12] Thomas Schweigler, Marek Gluza, Mohammadamin Tajik, Spyros Sotiriadis, Federica Cataldini, Si-Cong Ji, Frederik S Møller, Joao Sabino, Bernhard Rauer, Jens Eisert, et al. “Decay and recurrence of non-Gaussian correlations in a quantum many-body system”. *Nat. Phys.* **17**, 559–563 (2021).
- [13] Jesús Cuevas-Maraver, Panayotis G Kevrekidis, and Floyd Williams. “The sine-Gordon model and its applications”. Volume 10. Springer International Publishing. (2014).
- [14] Thorsten Schumm, S Hofferberth, L Mauritz Andersson, Stefan Wildermuth, Steffen Groth, Israel Bar-Joseph, Jörg Schmiedmayer, and Peter Krüger. “Matter-wave interferometry in a double well on an atom chip”. *Nat. Phys.* **1**, 57–62 (2005).
- [15] S Hofferberth, Igor Lesanovsky, Thorsten Schumm, A Imambekov, V Gritsev, E Demler, and Jörg Schmiedmayer. “Probing quantum and thermal noise in an interacting many-body system”. *Nat. Phys.* **4**, 489–495 (2008).
- [16] S Hofferberth, Igor Lesanovsky, B Fischer, Thorsten Schumm, and Jörg Schmiedmayer. “Non-equilibrium coherence dynamics in one-dimensional Bose gases”. *Nature* **449**, 324–327 (2007).
- [17] Michael Gring, Maximilian Kuhnert, Tim Langen, Takuya Kitagawa, Bernhard Rauer, Matthias Schreitl, Igor Mazets, D Adu Smith, Eugene Demler, and Jörg Schmiedmayer. “Relaxation and prethermalization in an isolated quantum system”. *Science* **337**, 1318–1322 (2012).
- [18] Bernhard Rauer, Sebastian Erne, Thomas Schweigler, Federica Cataldini, Mohammadamin Tajik, and Jörg Schmiedmayer. “Recurrences in an isolated quantum many-body system”. *Science* **360**, 307–310 (2018).
- [19] Mohammadamin Tajik, Ivan Kukuljan, Spyros Sotiriadis, Bernhard Rauer, Thomas Schweigler, Federica Cataldini, João Sabino, Frederik Møller, Philipp Schüttelkopf, Si-Cong Ji, et al. “Verification of the area law of mutual information in a quantum field simulator”. *Nat. Phys.* (2023).
- [20] S Hofferberth, Igor Lesanovsky, B Fischer, J Verdu, and Jörg Schmiedmayer. “Radiofrequency-dressed-state potentials for neutral atoms”. *Nat. Phys.* **2**, 710–716 (2006).
- [21] Mohammadamin Tajik, Bernhard Rauer, Thomas Schweigler, Federica Cataldini, João Sabino, Frederik S Møller, Si-Cong Ji, Igor E Mazets, and Jörg

- Schmiedmayer. “Designing arbitrary one-dimensional potentials on an atom chip”. *Opt. Express* **27**, 33474–33487 (2019).
- [22] Yevhenii Kuriatnikov, Nikolaus Würkner, Karthikeyan Kumaran, Tiantian Zhang, M. Venkat Ramana, Andreas Kugi, Jörg Schmiedmayer, Andreas Deutschmann-Olek, and Maximilian Prüfer. “Fast Coherent Splitting of Bose-Einstein Condensates” (2025). [arXiv:2507.06799](https://arxiv.org/abs/2507.06799).
- [23] M Gluza, T Schweigler, B Rauer, C Krumnow, J Schmiedmayer, and J Eisert. “Quantum read-out for cold atomic quantum simulators”. *Commun. Phys.* **3**, 12 (2020).
- [24] Marek Gluza, Thomas Schweigler, Mohammadamin Tajik, João Sabino, Federica Cataldini, Frederik Skovbo Møller, Si-Cong Ji, Bernhard Rauer, Jörg Schmiedmayer, Jens Eisert, et al. “Mechanisms for the emergence of Gaussian correlations”. *SciPost Phys.* **12**, 113 (2022).
- [25] Stefan Aimet, Mohammadamin Tajik, Gabrielle Tournaire, Philipp Schüttelkopf, João Sabino, Spyros Sotiriadis, Giacomo Guarnieri, Jörg Schmiedmayer, and Jens Eisert. “Experimentally probing Landauer’s principle in the quantum many-body regime”. *Nat. Phys.* (2025).
- [26] G. Vidal, J. I. Latorre, E. Rico, and A. Kitaev. “Entanglement in quantum critical phenomena”. *Phys. Rev. Lett.* **90**, 227902 (2003).
- [27] Nicolas Laflorencie, Erik S. Sørensen, Ming-Shyang Chang, and Ian Affleck. “Boundary Effects in the Critical Scaling of Entanglement Entropy in 1D Systems”. *Phys. Rev. Lett.* **96**, 100603 (2006).
- [28] Pasquale Calabrese and Alexandre Lefevre. “Entanglement spectrum in one-dimensional systems”. *Phys. Rev. A* **78**, 032329 (2008).
- [29] Pasquale Calabrese and John Cardy. “Entanglement entropy and conformal field theory”. *J. Phys. A: Math. Theor.* **42**, 504005 (2009).
- [30] J. Eisert, M. Cramer, and M. B. Plenio. “Colloquium: Area laws for the entanglement entropy”. *Rev. Mod. Phys.* **82**, 277–306 (2010).
- [31] Pasquale Calabrese, Mihail Mintchev, and Ettore Vicari. “The entanglement entropy of one-dimensional systems in continuous and homogeneous space”. *J. Stat. Mech.* **2011**, P09028 (2011).
- [32] M. Kuhnert, R. Geiger, T. Langen, M. Gring, B. Rauer, T. Kitagawa, E. Demler, D. Adu Smith, and J. Schmiedmayer. “Multimode dynamics and emergence of

- a characteristic length scale in a one-dimensional quantum system”. *Phys. Rev. Lett.* **110**, 090405 (2013).
- [33] Tim Langen, Remi Geiger, Maximilian Kuhnert, Bernhard Rauer, and Joerg Schmiedmayer. “Local emergence of thermal correlations in an isolated quantum many-body system”. *Nat. Phys.* **9**, 640–643 (2013).
 - [34] Tim Langen, Sebastian Erne, Remi Geiger, Bernhard Rauer, Thomas Schweigler, Maximilian Kuhnert, Wolfgang Rohringer, Igor E Mazets, Thomas Gasenzer, and Jörg Schmiedmayer. “Experimental observation of a generalized Gibbs ensemble”. *Science* **348**, 207–211 (2015).
 - [35] D Adu Smith, Michael Gring, Tim Langen, Maximilian Kuhnert, Bernhard Rauer, Remi Geiger, Takuya Kitagawa, Igor Mazets, Eugene Demler, and Jörg Schmiedmayer. “Prethermalization revealed by the relaxation dynamics of full distribution functions”. *New J. Phys.* **15**, 075011 (2013).
 - [36] Tiantian Zhang, Mira Maiwöger, Filippo Borselli, Yevhenii Kuriatnikov, Jörg Schmiedmayer, and Maximilian Prüfer. “Squeezing Oscillations in a Multimode Bosonic Josephson Junction”. *Phys. Rev. X* **14**, 011049 (2024).
 - [37] Maximilian Prüfer, Yuri Minoguchi, Tiantian Zhang, Yevhenii Kuriatnikov, M. Venkat Ramana, and Jörg Schmiedmayer. “Quantum-Limited Generalized Measurement for Tunnel-Coupled Condensates”. *Phys. Rev. Lett.* **133**, 250403 (2024).
 - [38] Taufiq Murtadho, Federica Cataldini, Sebastian Erne, Marek Gluza, Mohammadamin Tajik, Jörg Schmiedmayer, and Nelly H. Y. Ng. “Measurement of total phase fluctuation in cold-atomic quantum simulators”. *Phys. Rev. Res.* **7**, L022031 (2025).
 - [39] Jan Sperling and Elizabeth Agudelo. “Entanglement of particles versus entanglement of fields: Independent quantum resources”. *Phys. Rev. A* **107**, 042420 (2023).
 - [40] Jérôme Martin and Vincent Vennin. “Real-space entanglement of quantum fields”. *Phys. Rev. D* **104**, 085012 (2021).
 - [41] Daniele Teresi and Giuseppe Compagno. “Entanglement between quantum fields” (2011). [arXiv:1012.3915](https://arxiv.org/abs/1012.3915).
 - [42] Ali Mollabashi, Noburo Shiba, and Tadashi Takayanagi. “Entanglement between

- two interacting CFTs and generalized holographic entanglement entropy”. *J. High Energ. Phys.* **2014**, 1–36 (2014).
- [43] Yuichiro Nakai, Noburo Shiba, and Masaki Yamada. “Entanglement entropy and decoupling in the universe”. *Phys. Rev. D* **96**, 123518 (2017).
 - [44] Didier Poilblanc. “Entanglement Spectra of Quantum Heisenberg Ladders”. *Phys. Rev. Lett.* **105**, 077202 (2010).
 - [45] Andreas M. Läuchli and John Schliemann. “Entanglement spectra of coupled $s = \frac{1}{2}$ spin chains in a ladder geometry”. *Phys. Rev. B* **85**, 054403 (2012).
 - [46] Xiao Chen and Eduardo Fradkin. “Quantum entanglement and thermal reduced density matrices in fermion and spin systems on ladders”. *J. Stat. Mech.* **2013**, P08013 (2013).
 - [47] Shunsuke Furukawa and Yong Baek Kim. “Entanglement entropy between two coupled Tomonaga-Luttinger liquids”. *Phys. Rev. B* **83**, 085112 (2011).
 - [48] Rex Lundgren, Yohei Fuji, Shunsuke Furukawa, and Masaki Oshikawa. “Entanglement spectra between coupled Tomonaga-Luttinger liquids: Applications to ladder systems and topological phases”. *Phys. Rev. B* **88**, 245137 (2013).
 - [49] Qiang Miao and Thomas Barthel. “Eigenstate entanglement: Crossover from the ground state to volume laws”. *Phys. Rev. Lett.* **127**, 040603 (2021).
 - [50] Eugenio Bianchi, Lucas Hackl, Mario Kieburg, Marcos Rigol, and Lev Vidmar. “Volume-law entanglement entropy of typical pure quantum states”. *PRX Quantum* **3**, 030201 (2022).
 - [51] Christophe Mora and Yvan Castin. “Extension of Bogoliubov theory to quasicondensates”. *Phys. Rev. A* **67**, 053615 (2003).
 - [52] Thomas Schweigler. “Correlations and dynamics of tunnel-coupled one-dimensional bose gases”. PhD thesis. Technische Universität Wien. (2019).
 - [53] Yuri Daniel van Nieuwkerk, Jörg Schmiedmayer, and Fabian Essler. “Projective phase measurements in one-dimensional Bose gases”. *SciPost Phys.* **5**, 046 (2018).
 - [54] Taufiq Murtadho, Marek Gluza, Khatee Zathul Arifa, Sebastian Erne, Jörg Schmiedmayer, and Nelly Huei Ying Ng. “Systematic analysis of relative phase extraction in one-dimensional Bose gases interferometry”. *SciPost Phys.* **18**, 065 (2025).

- [55] Mohammadamin Tajik, Marek Gluza, Nicolas Sebe, Philipp Schüttelkopf, Federica Cataldini, João Sabino, Frederik Møller, Si-Cong Ji, Sebastian Erne, Giacomo Guarnieri, et al. “Experimental observation of curved light-cones in a quantum field simulator”. PNAS **120**, e2301287120 (2023).
- [56] Dmitry Sergeevich Petrov. “Bose-Einstein condensation in low-dimensional trapped gases”. PhD thesis. Universiteit van Amsterdam [Host]. (2003).
- [57] Nicholas K. Whitlock and Isabelle Bouchoule. “Relative phase fluctuations of two coupled one-dimensional condensates”. Phys. Rev. A **68**, 053609 (2003).
- [58] Alessio Serafini. “Quantum continuous variables: a primer of theoretical methods”. CRC press. (2017).
- [59] R. Simon. “Peres-Horodecki Separability Criterion for Continuous Variable Systems”. Phys. Rev. Lett. **84**, 2726–2729 (2000).
- [60] M. B. Plenio. “Logarithmic negativity: A full entanglement monotone that is not convex”. Phys. Rev. Lett. **95**, 090503 (2005).
- [61] Lu-Ming Duan, G. Giedke, J. I. Cirac, and P. Zoller. “Inseparability criterion for continuous variable systems”. Phys. Rev. Lett. **84**, 2722–2725 (2000).
- [62] R. F. Werner and M. M. Wolf. “Bound Entangled Gaussian States”. Phys. Rev. Lett. **86**, 3658–3661 (2001).
- [63] Remi Geiger, Tim Langen, IE Mazets, and Jörg Schmiedmayer. “Local relaxation and light-cone-like propagation of correlations in a trapped one-dimensional Bose gas”. New J. Phys. **16**, 053034 (2014).
- [64] L. Foini and T. Giamarchi. “Nonequilibrium dynamics of coupled luttinger liquids”. Phys. Rev. A **91**, 023627 (2015).
- [65] Yuri Daniel van Nieuwkerk, Jörg Schmiedmayer, and Fabian Essler. “Josephson oscillations in split one-dimensional bose gases”. SciPost Physics **10**, 090 (2021).
- [66] Kenneth Maussang, G. Edward Marti, Tobias Schneider, Philipp Treutlein, Yun Li, Alice Sinatra, Romain Long, Jérôme Estève, and Jakob Reichel. “Enhanced and Reduced Atom Number Fluctuations in a BEC Splitter”. Phys. Rev. Lett. **105**, 080403 (2010).
- [67] T. Berrada, S. van Frank, R. Bückner, T. Schumm, J. F. Schaff, and J. Schmiedmayer. “Integrated Mach-Zehnder interferometer for Bose-Einstein condensates”. Nat. Commun. **4**, 2077 (2013).

- [68] Marios H. Michael, Jörg Schmiedmayer, and Eugene Demler. “From the moving piston to the dynamical casimir effect: Explorations with shaken condensates”. *Phys. Rev. A* **99**, 053615 (2019).
- [69] Adilet Imambekov and Leonid I Glazman. “Universal theory of nonlinear Luttinger liquids”. *Science* **323**, 228–231 (2009).
- [70] Adilet Imambekov, Thomas L. Schmidt, and Leonid I. Glazman. “One-dimensional quantum liquids: Beyond the Luttinger liquid paradigm”. *Rev. Mod. Phys.* **84**, 1253–1306 (2012).
- [71] Takuya Kitagawa, Adilet Imambekov, Jörg Schmiedmayer, and Eugene Demler. “The dynamics and prethermalization of one-dimensional quantum systems probed through the full distributions of quantum noise”. *New J. Phys.* **13**, 073018 (2011).
- [72] J. Berges, Sz. Borsányi, and C. Wetterich. “Prethermalization”. *Phys. Rev. Lett.* **93**, 142002 (2004).
- [73] Takashi Mori, Tatsuhiko N Ikeda, Eriko Kaminishi, and Masahito Ueda. “Thermalization and prethermalization in isolated quantum systems: a theoretical overview”. *J. Phys. B* **51**, 112001 (2018).
- [74] Marcos Rigol, Vanja Dunjko, Vladimir Yurovsky, and Maxim Olshanii. “Relaxation in a Completely Integrable Many-Body Quantum System: An Ab Initio Study of the Dynamics of the Highly Excited States of 1D Lattice Hard-Core Bosons”. *Phys. Rev. Lett.* **98**, 050405 (2007).
- [75] H.-P. Stimming, N. J. Mauser, J. Schmiedmayer, and I. E. Mazets. “Dephasing in coherently split quasicondensates”. *Phys. Rev. A* **83**, 023618 (2011).
- [76] IE Mazets and J Schmiedmayer. “Dephasing in two decoupled one-dimensional Bose-Einstein condensates and the subexponential decay of the interwell coherence”. *Eur. Phys. J. B* **68**, 335–339 (2009).
- [77] Maximilian Kuhnert. “Thermalization and Prethermalization in an Ultracold Bose Gas”. PhD thesis. Technische Universität Wien. (2013).
- [78] Federica Cataldini, Frederik Møller, Mohammadamin Tajik, João Sabino, Si-Cong Ji, Igor Mazets, Thomas Schweigler, Bernhard Rauer, and Jörg Schmiedmayer. “Emergent Pauli Blocking in a Weakly Interacting Bose Gas”. *Phys. Rev. X* **12**, 041032 (2022).

- [79] A. A. Burkov, M. D. Lukin, and Eugene Demler. “Decoherence dynamics in low-dimensional cold atom interferometers”. *Phys. Rev. Lett.* **98**, 200404 (2007).
- [80] Sebastian Huber, Michael Buchhold, Jörg Schmiedmayer, and Sebastian Diehl. “Thermalization dynamics of two correlated bosonic quantum wires after a split”. *Phys. Rev. A* **97**, 043611 (2018).
- [81] Amaury Micheli and Scott Robertson. “Phonon decay in one-dimensional atomic Bose quasicondensates via Beliaev-Landau damping”. *Phys. Rev. B* **106**, 214528 (2022).
- [82] Tim Langen, Thomas Gasenzer, and Jörg Schmiedmayer. “Prethermalization and universal dynamics in near-integrable quantum systems”. *J. Stat. Mech.* **2016**, 064009 (2016).
- [83] Andreas Winter. “Tight uniform continuity bounds for quantum entropies: conditional entropy, relative entropy distance and energy constraints”. *Commun. Math. Phys.* **347**, 291–313 (2016).

Appendix A. Derivation of logarithmic negativity and mutual information for tunnel-coupled gases in equilibrium

From the expressions of the Bogoliubov decomposition of the fields in the symmetric (+) and antisymmetric (−) basis [Eqs. (18) and (19)] one can obtain analytical formula for all elements of the covariance matrix (Γ) in A, B basis as follows

$$\langle \hat{\phi}_k^a \hat{\phi}_k^b \rangle = \begin{cases} \frac{1}{8n_{1D}} \left(\frac{\varepsilon_k^+}{E_k} (1 + 2\eta_k^+) + \frac{\varepsilon_k^-}{E_k + 2\hbar J} (1 + 2\eta_k^-) \right) & \text{if } a = b \\ \frac{1}{8n_{1D}} \left(\frac{\varepsilon_k^+}{E_k} (1 + 2\eta_k^+) - \frac{\varepsilon_k^-}{E_k + 2\hbar J} (1 + 2\eta_k^-) \right) & \text{if } a \neq b, \end{cases} \quad (\text{A.1})$$

$$\langle \delta \hat{n}_k^a \delta \hat{n}_k^b \rangle = \begin{cases} \frac{n_{1D}}{2} \left(\frac{E_k}{\varepsilon_k^+} (1 + 2\eta_k^+) + \frac{E_k + 2\hbar J}{\varepsilon_k^-} (1 + 2\eta_k^-) \right) & \text{if } a = b \\ \frac{n_{1D}}{2} \left(\frac{E_k}{\varepsilon_k^+} (1 + 2\eta_k^+) - \frac{E_k + 2\hbar J}{\varepsilon_k^-} (1 + 2\eta_k^-) \right) & \text{if } a \neq b, \end{cases} \quad (\text{A.2})$$

and all other elements are zeros. Note that the covariance matrix Γ is non-diagonal, it has non-zero elements corresponding to $a \neq b$.

We first derive the formula for the logarithmic negativity $E_{\mathcal{N}}$ [Eq. (21)]. We start by performing partial transposition $\Gamma^{\top B}$, which in our case corresponds to the transformation $\langle \hat{\phi}_k^A \hat{\phi}_k^B \rangle \rightarrow -\langle \hat{\phi}_k^A \hat{\phi}_k^B \rangle$. Next, we need to evaluate the symplectic eigenvalues of $\Gamma^{\top B}$ defined by the positive eigenvalues of $i(\Omega \oplus \Omega)\Gamma^{\top B}$. This can be analytically done by first applying a symplectic transformation

$$\tilde{\Gamma}^{\top B} = \mathcal{S} \Gamma^{\top B} \mathcal{S}^{\top} \quad \text{with} \quad \mathcal{S} = \frac{1}{\sqrt{2}} \begin{pmatrix} I_{2\Lambda} & I_{2\Lambda} \\ I_{2\Lambda} & -I_{2\Lambda} \end{pmatrix}. \quad (\text{A.3})$$

The transformation \mathcal{S} preserves the symplectic structure $\mathcal{S}(\Omega \oplus \Omega)\mathcal{S}^T = \Omega \oplus \Omega$ and thus leaves the symplectic eigenvalues invariant. Meanwhile, the transformed matrix $\tilde{\Gamma}^{\top B}$ takes a diagonal form. For a diagonal covariance matrix, Schur's determinant formula allows us to write the symplectic eigenvalues as the square root of the product of the diagonal elements in each quadrature. In our context, they are given by

$$\nu_k^{\pm} \Big|_{\Gamma^{\top B}} = \sqrt{(\langle \hat{\phi}_k^A \hat{\phi}_k^A \rangle \mp \langle \hat{\phi}_k^A \hat{\phi}_k^B \rangle)(\langle \delta \hat{n}_k^A \delta \hat{n}_k^A \rangle \pm \langle \delta \hat{n}_k^A \delta \hat{n}_k^B \rangle)} \quad (\text{A.4})$$

$$= \frac{1}{2} \sqrt{(1 + 2\eta_k^+)(1 + 2\eta_k^-)} \left[\frac{\varepsilon_k^-}{\varepsilon_k^+} \frac{E_k}{E_k + 2\hbar J} \right]^{\pm 1/2}. \quad (\text{A.5})$$

Entanglement is detected by logarithmic negativity if $\Gamma^{\top B}$ violates the Heisenberg uncertainty principle, i.e. either $\nu_k^+ < 1/2$ or $\nu_k^- < 1/2$ [See Eq. (16)]. Meanwhile,

one can check from Eq. (A.5) that $\nu_k^- \geq 1/2$ by noticing that

$$\left[\frac{\varepsilon_k^-}{\varepsilon_k^+} \frac{E_k}{E_k + 2\hbar J} \right]^{-1/2} = \sqrt{\frac{(E_k + 2\hbar J)(E_k + 2gn_{1D})}{E_k(E_k + 2\hbar J + 2gn_{1D})}} \geq 1, \quad (\text{A.6})$$

and $\sqrt{(1 + 2\eta_k^+)(1 + 2\eta_k^-)} \geq 1$. Hence, only ν_k^+ contribute to the logarithmic negativity. By substituting ν_k^+ from Eq. (A.5) to Eq. (16) we recover Eq. (21) in the main text. The expression for the threshold temperature [Eq. (23)] is obtained by setting $\nu_k^+ = 1/2$.

The derivation for mutual information $I(A : B)$ [Eq. (24)] proceeds in a similar way. We first compute the symplectic eigenvalues λ_k of the diagonal reduced covariance matrix $\Gamma^{AA} = \Gamma^{BB}$. For $a \in \{A, B\}$ we find

$$\lambda_k \Big|_{\Gamma^{aa}} = \sqrt{\langle \hat{\phi}_k^a \hat{\phi}_k^a \rangle \langle \delta \hat{n}_k^a \delta \hat{n}_k^a \rangle} \quad (\text{A.7})$$

$$= \frac{1}{4} \sqrt{[(1 + 2\eta_k^+) + C_k(1 + 2\eta_k^-)] [(1 + 2\eta_k^+) + C_k^{-1}(1 + 2\eta_k^-)]}, \quad (\text{A.8})$$

where $C_k = (\varepsilon_k^- / \varepsilon_k^+)(E_k / (E_k + 2\hbar J))$. Then, for calculating the symplectic spectrum of the joint covariance matrix Γ , we perform the symplectic transformation (A.3) to Γ and obtain the symplectic eigenvalues σ_k^\pm

$$\sigma_k^\pm \Big|_{\Gamma} = \left(\eta_k^\pm + \frac{1}{2} \right) \quad (\text{A.9})$$

Using the definition of mutual information and the formula for the von-Neumann entropy [Eqs. (17) and (15)] we recover the result for the mutual information in Eq. (24).

Appendix B. Derivation of logarithmic negativity and mutual information for coherently split gases

Immediately after the coherent splitting, we assume thermal occupation in the symmetric sector and squeezed quantum noise in the antisymmetric sector [Eq. (26)]. The covariance matrix elements are now expressed as

$$\langle \hat{\phi}_k^a \hat{\phi}_k^b \rangle = \begin{cases} \frac{1}{4n_{1D}r^2} \left[\frac{r^2}{2} \frac{\varepsilon_k^+}{E_k} (1 + 2\eta_k^+) + 1 \right] & \text{if } a = b \\ \frac{1}{4n_{1D}r^2} \left[\frac{r^2}{2} \frac{\varepsilon_k^+}{E_k} (1 + 2\eta_k^+) - 1 \right] & \text{if } a \neq b, \end{cases} \quad (\text{B.1})$$

$$\langle \delta \hat{n}_k^a \delta \hat{n}_k^b \rangle = \begin{cases} \frac{n_{1D} r^2}{4} \left[\frac{E_k}{\varepsilon_k^+} \frac{2}{r^2} (1 + 2\eta_k^+) + 1 \right] & \text{if } a = b \\ \frac{n_{1D} r^2}{4} \left[\frac{E_k}{\varepsilon_k^+} \frac{2}{r^2} (1 + 2\eta_k^+) - 1 \right] & \text{if } a \neq b, \end{cases} \quad (\text{B.2})$$

and all other elements are zeros. Since the covariance matrix Γ has the same structure as in Eq. (A.1) and (A.2), the calculation done in Appendix A can be extended to the split case.

The symplectic eigenvalues for the partially transposed covariance matrix are calculated to be

$$\nu_k^+ \Big|_{\Gamma^{\top_B}} = \frac{1}{r} \sqrt{\frac{E_k}{\varepsilon_k^+} \left(\eta_k^+ + \frac{1}{2} \right)} \quad \nu_k^- \Big|_{\Gamma^{\top_B}} = \frac{r}{2} \sqrt{\frac{\varepsilon_k^+}{E_k} \left(\eta_k^+ + \frac{1}{2} \right)}. \quad (\text{B.3})$$

Meanwhile, the symplectic eigenvalues of Γ^{aa} ($a \in \{A, B\}$) and Γ are

$$\lambda_k \Big|_{\Gamma^{aa}} = \frac{1}{4} \sqrt{(1 + 2\eta_k + \mathcal{C}_k) (1 + 2\eta_k + \mathcal{C}_k^{-1})} \quad \mathcal{C}_k = \frac{r^2}{2} \frac{\varepsilon_k}{E_k} \quad (\text{B.4})$$

$$\sigma_k^+ \Big|_{\Gamma} = \frac{1}{2} (1 + 2\eta_k) \quad \sigma_k^- \Big|_{\Gamma} = 0 \quad (\text{B.5})$$

From Eqs. (B.3)-(B.5) one can easily obtain the expression for logarithmic negativity and mutual information after coherent splitting [Eqs. (27) and (29)].

The formula for the threshold temperature [Eq. (28)] is obtained by finding the root to

$$\left(\nu_k^+ - \frac{1}{2} \right) \left(\nu_k^- - \frac{1}{2} \right) = 0. \quad (\text{B.6})$$

Recall that entanglement occurs when the partially transposed covariance matrix violates the Heisenberg uncertainty principle, i.e., either $\nu_k^+ < 1/2$ or $\nu_k^- < 1/2$. For the threshold temperature, we want to find a solution where at least one of them is exactly $1/2$.

After substituting Eq. (B.3) to Eq. (B.6), the problem is reduced to solving

$$x^2 = \frac{1}{2} (x - 1)(x + 1) F(k, r) \quad (\text{B.7})$$

where $x = \exp(\varepsilon_k^+ / (k_B T^*))$ and $F(k, r) = 1 + \frac{r^2}{4} \frac{\varepsilon_k^+}{E_k} + \frac{1}{r^2} \frac{E_k}{\varepsilon_k^+}$. The threshold temperature is thus obtained by $T^* = (k_B / \varepsilon_k^+) \ln x$ and x is the solution to Eq. (B.7).